


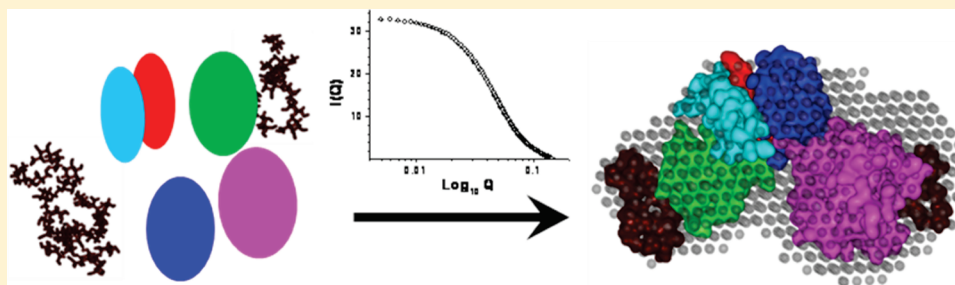
First Structural Model of Full-Length Human Tissue-Plasminogen Activator: A SAXS Data-Based Modeling Study

Yogendra S. Rathore,[†] Mohammad Rehan,[†] Kalpana Pandey, Girish Sahni, and Ashish*

Department of Protein Science and Engineering, Institute Of Microbial Technology (CSIR), Chandigarh, India 160036

 Supporting Information

ABSTRACT:



Human tissue-plasminogen activator (t-PA) is a multidomain glycoprotein which holds high biomedical value due to its therapeutic role in clot-specific fibrinolysis. Although atomic-resolution structures of individual domains except Kringle1 are available, no structural information is available on how these domains and glycosylation are oriented in space relative to each other in the full-length protein. SAXS intensity profile acquired from samples of t-PA was used to “steer” structures of individual domains and the homology model of the first kringle domain to generate a structural model of the protein part of t-PA. Differences in the shape profiles of SAXS data-based dummy atom and proteinogenic models aided in grafting glycosylated moieties on the coordinates of t-PA. According to previously reported mutagenesis-rendered altered functional profiles, normal-mode analysis of our model revealed that the fibrin binding F/E domains “communicate” with the active-site in the P domain via Kringle2, while Kringle1 is positioned away from these long-distance interactions.

INTRODUCTION

Structural insight on the full length human tissue plasminogen activator (t-PA) can play a critical role in initiating rational design of variants of this protease with altered or improved functions/specificities. t-PA is a thrombolytic serine protease which binds to zymogen plasminogen on the surface of fibrin and converts it into the active proteinase plasmin, which in turn clears the fibrin clot.¹ In the presence of cofactor fibrin, the enzymatic activity of the t-PA increases by several orders of magnitude.² The fibrin-specific activation of plasminogen has identified use of t-PA in the treatment of acute myocardial infarction, deep vein thrombosis, pulmonary embolism, and other thrombolytic disorders.³ The human t-PA comprising of 527 amino acids is synthesized and secreted as single-chain glycoprotein (molecular mass ~70 kDa) into the blood circulation by endothelial cells.⁴ There are three potential N-glycosylation sites at Asn¹¹⁷, Asn¹⁸⁴, and Asn⁴⁴⁸ which substantially decrease circulation lifetime of this protein due to receptor-mediated clearance in hepatocyte cells.^{5,6} In human and recombinant mammalian cell lines, a mixture of two isoforms of this protein with differential core glycosylation has been reported.⁷ Type I t-PA contains the glycosylation at all three sequons, whereas type II form lacks modifications at Asn¹⁸⁴. Interestingly, the glycosylation at Asn¹¹⁷ and Asn⁴⁴⁸ plays an

important regulatory role in clot lysis by substantially decreasing the fibrin binding and plasminogen activation in the absence of a fibrin clot.^{8,9} Upon activation on the fibrin clot, plasmin cleaves the t-PA at the scissile peptide bond, namely Arg²⁷⁵-Ile²⁷⁶ via limited proteolysis and converts the one-chain t-PA into the catalytically more active two-chain t-PA. This two chain t-PA contains a heavy N-terminal chain of 39 kDa and a C-terminal lighter segment of 33 kDa, which remain connected by one inter-chain disulfide bond.¹⁰

Like most other fibrinolytic and coagulation proteins, the full length t-PA contains multiple domains: (1) F domain (residues 4–50); (2) E domain (residues 51–87); (3) kringle domains [K1 domain (residues 88–175) and K2 domain (residues 176–256)], and (4) P domain/catalytic domain (residues 256–527) with His³²², Asp³⁷¹, and Ser⁴⁷⁸ as active site residues.¹¹ Moreover, it is known that the correctly folded and functional t-PA contains 17 intradomain disulfide bonds which are also present in the proteolytically cleaved active t-PA.¹⁰ Although, a number of t-PA derivatives with improved potential have been reported,^{2,12,13}

Received: July 29, 2011

Revised: November 28, 2011

Published: November 30, 2011

an insight into the structure–function relationship is still eluding. Prime limitation is unavailability of a structure of full-length t-PA either from X-ray diffraction or NMR or electron microscopy. As of now, structures of individual domains of t-PA except the K1 domain have been resolved in their unglycosylated forms by X-ray crystallography and NMR.^{14–20} With a long-term goal of rationally evolving different versions of t-PA with altered specificities, we used SAXS intensity data from a sample of t-PA to orient these domains relative to each other in space and rationally attach glycosylation moieties on the K1 and P domains. This work led to the first structural model of full-length t-PA which helped to answer how fibrin binding motifs in the N-terminal of this molecule can communicate with exosites surrounding the active-site in the C-terminal catalytic domain.

MATERIALS AND METHODS

t-PA Sample for SAXS Experiments. Recombinant human t-PA (Actilyse, Boehringer Ingelheim GmbH & Co. KG, Germany) used for treating stroke patients was purchased and resuspended in sterile water. To remove formulation ingredients, the protein sample was subjected to dialysis against PBS buffer, pH 7.2 (four changes of 45–90 min and final overnight). Postdialysis, t-PA was purified by size-exclusion chromatography using a Superdex 200 column attached to AKTA Explorer FPLC system (GE Life Sciences). A slightly diffused band about 65–67 kDa in 12% SDS-PAGE with reducing buffer helped in ascertaining the purity of the fraction collected from FPLC and that it is free from any degradation products (Supporting Information Figure 1). Similarly, the MALDI-TOF analysis of the sample used for structure analysis showed a major peak around 63.6 kDa (Voyager 4402, Applied Biosystems, Carlsbad, CA) (Supporting Information Figure 1). The final concentration of the protein was determined by UV–vis spectrophotometer using A_{280} (1 mg/mL) = 1.8.

SAXS Data Acquisition. SAXS data was collected on three samples of t-PA varying in their concentration from 0.8 to 0.3 mg/mL at X9 beamline (National Synchrotron Light Source, Brookhaven National Laboratory, Upton, NY). Using the automated sample loader and capillary cleaner system, for each experiment using about 90 μ L of sample and matched buffer, SAXS images were acquired thrice for 15 s each while flowing the sample (60 μ L/min) through a quartz flow cell. The samples waiting to be loaded and the manifold holding the capillary were maintained at 10 °C with a water bath. The scattered X-rays were recorded on charge-coupled device (CCD), corrected for flares close to beam-stopper, and circularly averaged about the coordinates of the main beam to obtain SAXS intensity profiles as a function of Q , using python script-based programs (written by Dr. Lin Yang, BNL). Three sets of data from the same sample were averaged. For each t-PA sample, the contribution from the buffer was subtracted to obtain the scattering intensity (I) from the protein sample as a function of momentum transfer vector, Q ($Q = [4\pi \sin \theta]/\lambda$), where λ is the beam wavelength and θ is the scattering angle. Immediately after data collection, samples were recovered in SDS-PAGE loading buffer. Similarity in the migration pattern of proteins collected after exposure to X-rays and the samples which remained in our lab confirmed that no sample underwent degradation during travel and/or radiation-induced damage during data collection (Supporting Information Figure 1A). Alongside, to calibrate beam intensity and estimate precise concentration of these proteins, we acquired SAXS data from a set of FPLC-purified proteins with previously determined

concentration: hen egg white lysozyme in sodium acetate buffer (14.2 kDa, Acros Organics),²¹ tetrameric form of GAPDH in phosphate buffer saline (147 kDa, Sigma Aldrich), and lactoferrin in phosphate buffer saline (80 kDa, Sigma Aldrich).

SAXS Data Analysis. Kratky plots [$I(Q) \times Q^2$ vs Q] of each data set were prepared to examine the globular vs Gaussian-chain-like nature of the protein molecules in solution. Guinier approximation for globular scattering species was employed to estimate the radius of gyration (R_G) of the protein molecules using only low Q data. As per this approximation, for a monodisperse sample of globular protein, a plot of $\ln I(Q)$ versus Q^2 , where $Q \times R_G \leq 1.3$, should be linear and fit into the following eq 1:

$$\ln[I(Q)] = \ln[I_0] - (R_G^2/3) \times Q^2 \quad (1)$$

Here, I_0 is defined as the intensity of scattering at zero angles and is directly proportional to the product of molar concentration and molecular mass of the scattering sample. Because of limitations of SAXS optics in direct and correct measurement of I_0 value, it can be approximated by extrapolating SAXS data to $Q \rightarrow 0$. R_G is defined as the root-mean-square of all elemental volumes from the center-of-mass of the particle to its edge, weighted by their scattering densities, and is characteristic of the overall shape of the molecule. The SAXS intensity profiles can also be processed presuming a rod-like shape of the scattering particles by using Guinier analysis for such particles (eq 2). The slope of this approximation computes the mean cross-sectional radius of the molecule, R_C , and the mean cross-sectional intensity at zero angle, $[I(Q)Q]_0$:

$$\ln[I(Q)Q] = \ln[(I(Q)Q)_0] - (R_C^2/2)Q^2 \quad (2)$$

Importantly, using R_G and R_C values, the length of an ellipsoidal structure, L , can be fairly estimated using the following relation-ships in eq 3:

$$L = [12(R_G^2 - R_C^2)]^{1/2} \quad (3)$$

For this study, both Guinier approximations were performed using the PRIMUS software package.²² Using GNOM45 software,²³ indirect Fourier transformation of the scattering data over the measured Q range computed a pairwise distribution function of interatomic vectors, $P(r)$ (eq 4).

$$P(r) = (1/2\pi) \int I(Q)Q \times r \sin(Q \times r) dQ \quad (4)$$

$P(r)$ is a histogram of the frequency of vector lengths connecting small volume elements within the entire volume of the scattering particle. The analysis also provided R_G and I_0 from the second moment and the start of $P(r)$, respectively.

Integrated Model Generation and Normal Mode Analysis.

To model the structure of proteinogenic portion of full-length t-PA, the following structures of different domains of t-PA available from X-ray crystallography and NMR in their unglycosylated forms were used: F and E domain (PDB ID: 1TPG), Kringle2 (PDB ID: 1TPK), and P domain (catalytic domain, PDB ID 1BDA). The unavailable structure of Kringle1 was generated by homology modeling using Swiss Modeler Server and the structure of Kringle2 as template (E -value $1.4e^{-15}$; PDB ID: 1PML chain A). SASREF program was used to position the individual domains relative to each other in space using measured SAXS $I(Q)$ profile as a reference.²⁴ Oligosaccharide moieties were attached at the N-glycosylation sites (Asn¹¹⁷ and Asn⁴⁴⁸) by

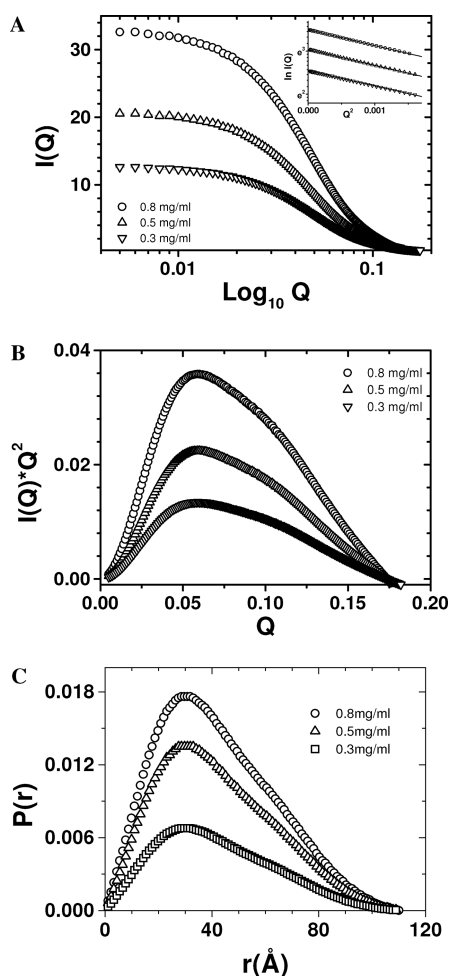


Figure 1. SAXS data analysis. (A) SAXS intensity profiles $I(Q)$ from samples of human t-PA are presented as a function of momentum transfer vector Q . Linear region of the Guinier analyses are presented in the inset. (B) Peak-like profile of the Kratky plots from individual SAXS data sets confirmed the globular nature of the protein molecules in solution. (C) $P(r)$ curves deduced for the t-PA molecules probably showing the presence of different interatomic vectors as a function of its dimension are shown here.

submitting the integrated model of the protein part of the t-PA to GlyProt server (<http://www.glycosciences.de/glyprot/>).²⁵ CRY SOL program was used to calculate theoretical SAXS profile of the computationally generated glycosylated and nonglycosylated models of t-PA and compare with the measured data.²⁶ Elastic network model was used to compute normal modes of vibrations accessible to this glycoprotein using ELNEMO server (<http://www.igs.cnrs-mrs.fr/elnetmo/>).²⁷ The five lowest frequency vibration modes were calculated using default values for perturbation.

Ab Initio Structure Restoration from SAXS Data. Employing dummy residues and constraints provided within the SAXS profile, the three-dimensional shape of the full-length protein was restored using the DAMMINQ program.²⁸ Ten individual models were generated for the glycoprotein without any predefined shape or symmetry bias using the Simulated Annealing-based convergence protocol. These individual solutions were averaged using the DAMAVER suite of programs to obtain a structural model that best represents the predominant shape of the t-PA molecules in solution.²⁹ For this protocol, ten calculations were performed using 660 dummy residues and a Fibonacci grid order of 15 (988 water molecules). SUPCOMB20 software was used to align the inertial axes of our SAXS-data based model and the SASREF generated model of t-PA in an automated manner.³⁰ Open source software such as SPDB viewer, PyMOL, and RASWIN 2.6UCB were used for graphical analysis and figure generation. Curve-fitting and data-plotting were performed using OriginLab software.

RESULTS AND DISCUSSION

SAXS Data Analysis. Upon comparing with the SDS-PAGE profiles published previously, the migration pattern of our t-PA in SDS-PAGE indicated that our samples predominantly contained the type II form of t-PA (Supporting Information Figure 1A).³¹ It is pertinent to mention here that as a source of protein, we used a formulation which is prescribed to patients, and type II possesses 2-fold more activity than its type I form. Fitting of the Gaussian distribution curve to the MALDI-TOF profile of the FPLC-purified protein sample indicated that t-PA molecules had a mass range of 63.6 ± 4.7 kDa (Supporting Information Figure 1B).

Table 1. Summary of Structural Parameters and Concentration of the t-PA Samples Computed from SAXS Data Analysis

Standard Proteins									
proteins	mass (kDa)	Guinier analysis			$P(r)$ analysis			concn(mg/mL)	$I_0/(c \cdot m)$
		R_G (Å)	R_C (Å)	L (Å)	D_{max} (Å)	R_G (Å)	I_0		
lysozyme	14.2	14.2	8.2	40.1	44	14.2	9.0	1 ^a	0.63
lactoferrin	77.2	29.6	10.3	96.1	98	29.7	39.1	0.8	0.64
GAPDH (Tetramer)	147	30.1	10.8	97.3	98	30.2	64.6	0.7	0.62
t-PA									
proteins	mass (kDa)	Guinier analysis			$P(r)$ analysis			concn(mg/mL)	actual concn(mg/mL)
		R_G (Å)	R_C (Å)	L (Å)	D_{max} (Å)	R_G (Å)	I_0		
sample 1	67	32.3 ± 0.1	15.1	100	110	33 ± 0.1	33.6	—	0.8
sample 2	67	32.2 ± 0.1	15.2	100	110	33 ± 0.1	21.0	—	0.5
sample 3	67	32.3 ± 0.3	15.2	100	110	33 ± 0.1	12.6	—	0.3

^a Extrapolated to a concentration of 1 mg/mL.

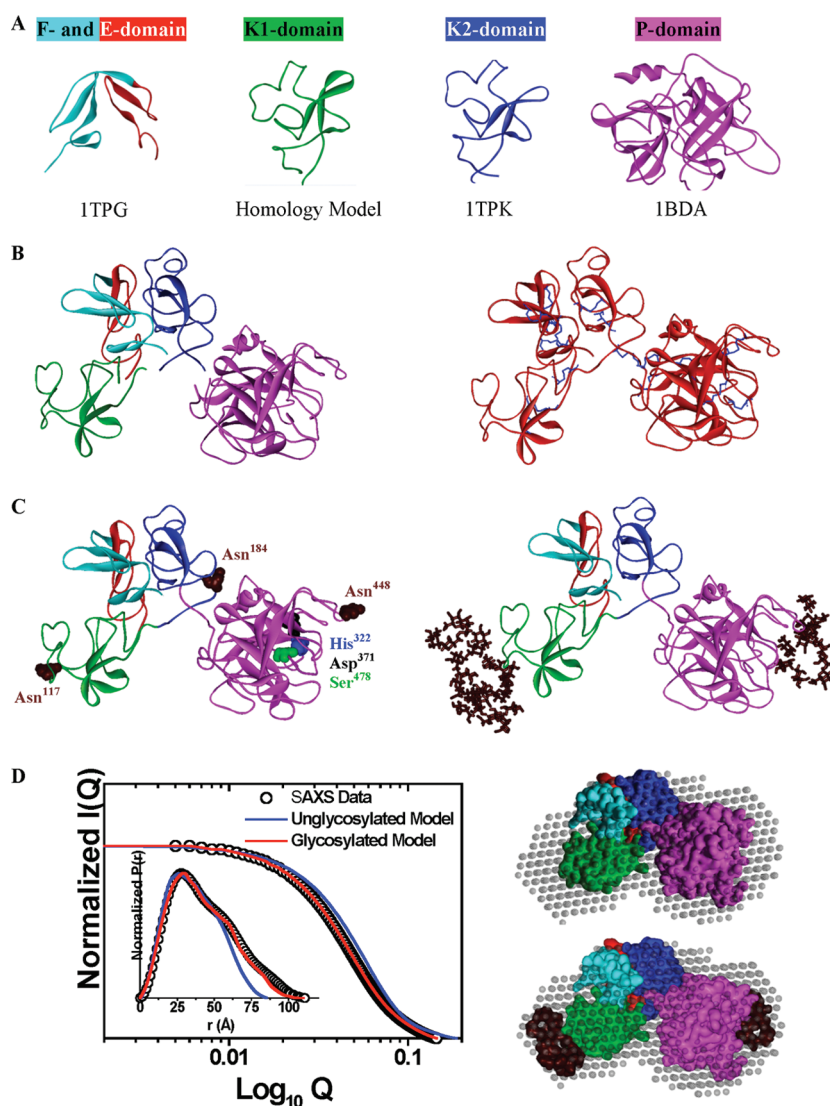


Figure 2. Generation of the composite model of the glycoprotein t-PA. (A) Structures of the individual domains used for generation of a total model of t-PA are presented here. The PDB IDs of the structures and the template used for modeling are mentioned below the structure. The color used to denote a certain domain has been retained throughout this work. (B) (Left) Relative positioning of the individual domains which best fitted the shape profile encoded in the measured SAXS data for the full-length protein. (Right) All 17 disulfide bonds (blue stick) essential for the functional form of t-PA were formed in our composite model created by manually interconnecting individual domains shown in the left panel. (C) While the left panel shows the three glycosylated sites in the continuous model of t-PA, the right panel includes the sugar moieties attached to protein coordinates as per mass and shape requirements: Asn¹¹⁷ and Asn⁴⁴⁸ (brown sticks). The active site residues His³²², Asp³⁷¹, and Ser⁴⁷⁸ in the catalytic domain are shown by blue, black, and green surfaces, respectively. (D) (Left) Comparison of the theoretical SAXS profile of the unglycosylated and glycosylated model of t-PA have been compared with the measured data. The inset shows the comparison of the $P(r)$ curves from the experimental data and from the theoretical SAXS profile of the models. (Right) Inertial axes of the unglycosylated (upper) and glycosylated (lower) models of t-PA aligned with the SAXS data-based dummy model (gray cpk) have been presented here.

The proteinogenic mass of t-PA molecules should be ~ 59 kDa, and the observed mass of 64–67 kDa from MALDI-TOF and SDS-PAGE suggests that the sugars comprise ~ 5 –8 kDa or 8–12% of molecular mass. The measured SAXS data from three samples of purified t-PA varying in concentration from 0.8 to 0.3 mg/mL is presented in Figure 1A. Peak-like profile of the Kratky plots of the intensity data confirmed a globular scattering nature of the protein molecules in solution (Figure 1B). The presence of a pronounced shoulder indicated a bilobal shape for this molecule. Guinier approximation for globular particles indicated that the predominant shape of t-PA is characterized by an R_G of about 32.3 Å (Table 1, Figure 1A inset). Alternatively,

presuming a rod-shape for this molecule, Guinier approximation implied an R_C value of ~ 15.2 Å. Using eq 3, analysis of only low Q data indicated the predominant length of the t-PA molecules in solution to be about 100 Å. Analysis of the $P(r)$ curve or distribution profile of interatomic vectors leading to measured SAXS data over a wider Q range of 0.01 – 0.25 Å^{−1} conveyed that the predominant solution shape of t-PA molecules can be characterized with a D_{\max} and R_G value of ~ 110 and 33 Å, respectively (Figure 1C, Table 1). Similar to Kratky plots, the peak and shoulder profile of $P(r)$ curves also supported a bilobal shape for t-PA. To estimate the protein concentrations accurately, we also ran a set of standard proteins which extrapolated that the I_0 value

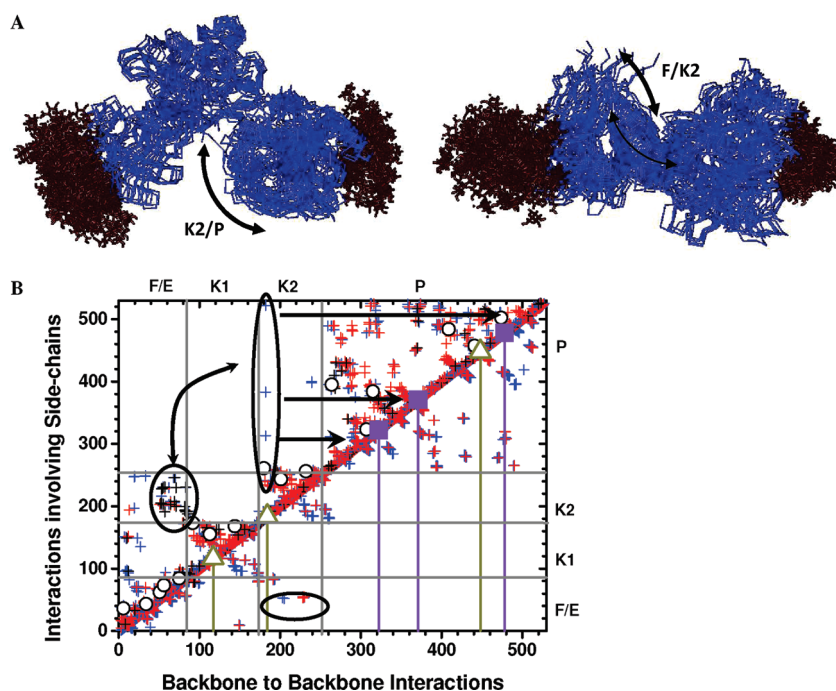


Figure 3. Normal mode calculation of the glycosylated model and analysis of collective motion. (A) The lowest frequency vibration mode representing the collective motions in the multidomain model of the glycoprotein, t-PA. Arrows highlight how F/E domains move toward K2 domain, which moves the K2 domain closer to the P domain. (B) The contact map is a way to represent collective motions of the residues in a two-dimensional manner. The red, blue, and black cross-hairs represent interactions within 2–3, 3–4, and 4–5 Å. Open circles represent the disulfide linkages. Dirty yellow open triangles and filled purple boxes with droplines represent the three glycosylation sites and three active site residues that are most important for protease activity, respectively. The black circles highlight residues involved in long-distance interactions.

for a proteinogenic mass of 1 kDa and at a concentration of ~ 1 mg/mL was about 0.6 au under the experimental conditions. This indicated that our protein samples had a concentration range of 0.8–0.3 mg/mL. As expected, similarity of structural parameters of the samples at this concentration range ruled out the presence of any kind of intermolecular effect for this glycoprotein.

Structural Model of t-PA. We used SAXS data for the sample with concentration ~ 0.8 mg/mL (as it had the best signal-to-noise ratio) to compute the full-length glycosylated model of human t-PA by automated positioning of the structures of individual domains in relative space. For the F–E domain, K2 domain, and P domain, their available crystal/NMR structures were utilized (Figure 2A). The unavailable structure of the K1 domain was modeled based on its high homology with the K2 domain (PDB ID: 1PML chain A). It is important to mention here that any residues present in the primary structure of t-PA but absent within the structural templates of domains were corrected. Defining the connectivity between individual domains and using the SASREF program, different relative positioning of these domains were tried until the theoretical SAXS profile of the three-dimensional ensemble compared well with the measured SAXS data (Supporting Information Figure 2 and Figure 2B). Comparison of the theoretical SAXS profile of the composite model of t-PA by positioning the domains in the three-dimensional space without defining domain connectivity to the experimentally measured data did not converge to low χ^2 values (Supporting Information Figure 2). Using the connectivity information based on primary structure and reducing the distance between contact points from 3 to 1.5 Å dramatically reduced the χ^2 values to about 3. Eventually, using the primary sequence and disconnected domains

model as template, we created a continuous model of t-PA (Figure 2B, right). In the process, some of the missing residues not resolved in the interdomain linkers were also modeled. The calculated structural model of the proteinogenic portion of full-length t-PA containing all the 17 disulfide linkages is shown in Figure 2B (right). To obtain a structural model of the glycoprotein, the composite model of the protein part was used for adding sugar moieties using the GlyProt server (Supporting Information Figure 3 and Figure 2C). Three glycosylation sites are known for t-PA: Asn¹¹⁷, Asn¹⁸⁴, and Asn⁴⁴⁸.⁷ When we tried to model sugar units on the protein chain of t-PA, we could succeed only at Asn¹¹⁷ and Asn⁴⁴⁸ because the Asn¹⁸⁴ was not surface accessible (Figure 2C). Importantly, the theoretical SAXS profile of the final glycosylated model of t-PA matched much better with the experimental data than the SAXS profile calculated from the unglycosylated model (Supporting Information Figure 4 and Figure 2D). This suggested that the glycosylated model computed by us is a good representation of the predominant global structure of type II t-PA molecule. Further, the area under the $P(r)$ curves calculated from the theoretical SAXS profile of the unglycosylated model was about 8% less than the area under the $P(r)$ curve computed for the glycosylated model (Figure 2D, left inset). Interestingly, this difference compares well with the mass of glycosylation on the type II form of t-PA. By aligning inertial axes of our SAXS data-based dummy atom model and models of unglycosylated and glycosylated models calculated for t-PA, we gained visual insight into how well the glycosylated model agreed with the SAXS data-based model (Figure 2D, right).

Previously, observations of the variable extent of glycosylation at Asn¹⁸⁴ were also attributed to differential accessibility of Asn¹⁸⁴ during post-translational processing events.³² Also, lesser activity

of the type I form of t-PA with glycosylation at Asn¹⁸⁴ has remained unexplained.³³ Our model of full-length t-PA protein suggests that the Asn¹⁸⁴ is “sandwiched” between the K2 and P domain in the folded protein (Figure 2C). If glycosylation events occur after formation of the disulfide linkages, the propensity of glycosylation at Asn¹⁸⁴ would be significantly reduced. Alternatively, if formation of disulfide linkages accompanies glycosylation, one would find a significant heterogeneity in the glycosylation at this site. In any case, we could successfully model glycosyl moieties at positions Asn¹¹⁷ and Asn⁴⁴⁸ with the sugar component having a mass of ~5 kDa, as expected for the functional or type II form of glycoprotein t-PA (Figure 2D).³⁴

Using the glycosylated model computed for t-PA, we were interested in mapping long-distance interactions which might be present in the molecule in a dynamic manner. To achieve this, we calculated lowest frequency vibration modes using the Elastic Network model. Analysis of the most collective perturbation conveyed that the F domain interacts with the K2 domain which in turn oscillates away or close to the P domain in a concerted fashion (Figure 3A). Mapping of the residues whose C α atoms vibrate in collective manner showed that the F/E domain skips interaction with the K1 domain and forms contacts directly with the K2 domain (Figure 3B). Previously it has also been reported that the functional potency of t-PA is predominantly mediated by the K2 domain followed by a lesser contribution of the F/E domain with almost no role for the K1 domain.³⁵ This probably occurs by virtue of the disulfide linkages which lock the K1 domain out of interaction, but the bulk mass of the K1 domain helps in sterically orienting F/E and K2 domains in proximity to each other in the tertiary structure. We hypothesize that these interactions seen in our composite model of t-PA represents some of the long-distance interactions which are integral to the substrate specificity of t-PA by activating the protease domain only when t-PA is bound to fibrin. Interestingly, residues 182–184 of the K2 domain seem to play a critical role in the relaying of communication between F and P domains as they interact with the F domain on one side, and on another side interact with residues which are in close proximity to the catalytic site formed by His³²², Ile³⁷¹, and Ser⁴⁷⁸. The importance of Asn¹⁸⁴ in enabling long-distance communication between fibrin-binding residues and the catalytic site further supports the notion that glycosylation at Asn¹⁸⁴ somehow insulates the long-distance communication between F and P domains. Overall, our work represents a classic case where SAXS intensity data has been employed to efficiently compose fragmented structures into a tertiary structural model which also validates the fibrin-mediated mechanism of t-PA activity hitherto unraveled through biochemical studies. This approach will be of particular advantage when seeking structural insight on multidomain proteins and/or glycoproteins which pose challenges in crystallization or study by NMR.

■ ASSOCIATED CONTENT

Supporting Information. SDS-PAGE and MALDI-TOF profiles of t-PA samples used for SAXS data collection and modeling, different computational models of t-PA using unglycosylated domains and the ASREF protocol, different glycosylated models for t-PA using SAXS data as structural constraints, and selection of relative orientations of sugar within the SAXS-based shape profile. This material is available free of charge via the Internet at <http://pubs.acs.org>.

■ AUTHOR INFORMATION

Corresponding Author

*Phone: 0172-6665295. Fax: 0172-2690632. E-mail: ashgang@imtech.res.in.

Author Contributions

[†]Contributed equally in this work.

■ ACKNOWLEDGMENT

The authors acknowledge financial support from CSIR (OLP-0056 and SIP-10). Y.S.R., M.R., and K.P. are grateful to UGC—CSIR and CSIR for research fellowships. Travel to the synchrotron was supported by CSIR-India. Use of the National Synchrotron Light Source, Brookhaven National Laboratory, was supported by the U.S. Department of Energy, Office of Science, Office of Basic Energy Sciences, under Contract No. DE-AC02-98CH10886.

■ REFERENCES

- (1) Hoylaerts, M.; Rijken, D. C.; Lijnen, H. R.; Collen, D. *J. Biol. Chem.* **1982**, *257*, 2912–2919.
- (2) Tachias, K.; Madison, E. L. *J. Biol. Chem.* **1995**, *270*, 18319–18322.
- (3) Collen, D.; Lijnen, H. R.; Todd, P. A.; Goa, K. L. *Drugs* **1989**, *38*, 346–388.
- (4) Rijken, D. C.; Wijngaards, G.; Welbergen, J. *Thromb. Res.* **1980**, *18*, 815–830.
- (5) Smith, R. A. *Biochem. J.* **1986**, *239*, 477–479.
- (6) Fuchs, H. E.; Berger, H., Jr.; Pizzo, S. V. *Blood* **1985**, *65*, 539–544.
- (7) Pohl, G.; Kallstrom, M.; Bergsdorf, N.; Wallen, P.; Jornvall, H. *Biochemistry* **1984**, *23*, 3701–3707.
- (8) Wittwer, A. J.; Howard, S. C.; Carr, L. S.; Harakas, N. K.; Feder, J.; Parekh, R. B.; Rudd, P. M.; Dwek, R. A.; Rademacher, T. W. *Biochemistry* **1989**, *28*, 7662–7669.
- (9) Hansen, L.; Blue, Y.; Barone, K.; Collen, D.; Larsen, G. R. *J. Biol. Chem.* **1988**, *263*, 15713–15719.
- (10) Pennica, D.; Holmes, W. E.; Kohr, W. J.; Harkins, R. N.; Vehar, G. A.; Ward, C. A.; Bennett, W. F.; Yelverton, E.; Seeburg, P. H.; Heyneker, H. L.; Goeddel, D. V.; Collen, D. *Nature* **1983**, *301*, 214–221.
- (11) Lijnen, H. R.; Collen, D. *Thromb. Haemostasis* **1991**, *66*, 88–110.
- (12) Keyt, B. A.; Paoni, N. F.; Refino, C. J.; Berleau, L.; Nguyen, H.; Chow, A.; Lai, J.; Pena, L.; Pater, C.; Ogez, J.; et al. *Proc. Natl. Acad. Sci. U.S.A.* **1994**, *91*, 3670–3674.
- (13) Mattes, R. *Semin. Thromb. Hemostasis* **2001**, *27*, 325–336.
- (14) Renatus, M.; Engh, R. A.; Stubbs, M. T.; Huber, R.; Fischer, S.; Kohnert, U.; Bode, W. *EMBO J.* **1997**, *16*, 4797–4805.
- (15) Downing, A. K.; Driscoll, P. C.; Harvey, T. S.; Dudgeon, T. J.; Smith, B. O.; Baron, M.; Campbell, I. D. *J. Mol. Biol.* **1992**, *225*, 821–833.
- (16) de Vos, A. M.; Ultsch, M. H.; Kelley, R. F.; Padmanabhan, K.; Tulinsky, A.; Westbrook, M. L.; Kossiakoff, A. A. *Biochemistry* **1992**, *31*, 270–279.
- (17) Byeon, I. J.; Llinas, M. *J. Mol. Biol.* **1991**, *222*, 1035–1051.
- (18) Smith, B. O.; Downing, A. K.; Driscoll, P. C.; Dudgeon, T. J.; Campbell, I. D. *Structure* **1995**, *3*, 823–833.
- (19) Lamba, D.; Bauer, M.; Huber, R.; Fischer, S.; Rudolph, R.; Kohnert, U.; Bode, W. *J. Mol. Biol.* **1996**, *58*, 117–135.
- (20) Renatus, M.; Stubbs, M. T.; Huber, R.; Bringmann, P.; Donner, P.; Schleuning, W. D.; Bode, W. *Biochemistry* **1997**, *36*, 13483–13493.
- (21) Ashish, Solanki, A. K.; Boone, C. D.; Krueger, J. K. *Biochem. Biophys. Res. Commun.* **2010**, *391*, 947–951.
- (22) Konarev, P. V.; Volkov, V. V.; Sokolova, A. V.; Koch, M. H. J.; Svergun, D. I. *J. Appl. Crystallogr.* **2003**, *36*, 1277–1282.
- (23) Svergun, D. I. *J. Appl. Crystallogr.* **1992**, *25*, 495–503.
- (24) Petoukhov, M. V.; Svergun, D. I. *Biophys. J.* **2005**, *89*, 1237–1250.

- (25) Bohne-Lang, A.; von der Lieth, C. W. *Nucleic Acids Res.* **2005**, *33*, W214–219.
- (26) Svergun, D.; Barberato, C.; Koch, M. H. J. *J. Appl. Crystallogr.* **1995**, *28*, 768–773.
- (27) Suhre, K.; Sanejouand, Y. H. *Nucleic Acids Res.* **2004**, *32*, W610–614.
- (28) Svergun, D. I. *Biophys. J.* **1999**, *76*, 2879–2886.
- (29) Volkov, V. V.; Svergun, D. I. *J. Appl. Crystallogr.* **2003**, *36*, 860–864.
- (30) Kozin, M. B.; Svergun, D. I. *J. Appl. Crystallogr.* **2001**, *34*, 33–41.
- (31) Mori, K.; Dwek, R. A.; Downing, A. K.; Opdenakker, G.; Rudd, P. M. *J. Biol. Chem.* **1995**, *270*, 3261–3267.
- (32) Allen, S.; Naim, H. Y.; Bulleid, N. J. *J. Biol. Chem.* **1995**, *270*, 4797–4804.
- (33) Einarsson, M.; Brandt, J.; Kaplan, L. *Biochim. Biophys. Acta* **1985**, *830*, 1–10.
- (34) Ranby, M.; Bergsdorf, N.; Pohl, G.; Wallen, P. *FEBS Lett.* **1982**, *146*, 289–292.
- (35) van Zonneveld, A. J.; Veerman, H.; Pannekoek, H. *Proc. Natl. Acad. Sci. U.S.A.* **1986**, *83*, 4670–4674.